Research Article

Shide Yu[#], Zhenyu Chen[#], Yiyin Sun[#], Dahong Huang^{*}, and Ting Sun^{*}

Effect of grain boundary segregation and oxygen vacancy annihilation on aging resistance of cobalt oxide-doped 3Y-TZP ceramics for biomedical applications

https://doi.org/10.1515/rams-2023-0159 received March 21, 2023; accepted December 04, 2023

Abstract: This study aims to investigate the diffusion stabilization process of nano-Co₂O₃ during the non-precursor transformation of 3Y-TZP. 3Y-TZP was set as the control group, and the experimental groups were 0.1-0.3 mol% nano-Co₂O₃-doped 3Y-TZP. The samples were prepared by the ball milling process, isostatic cool pressing, and sintering. All samples were hydrothermally treated at 134°C and 2 bar for different time periods. The resistance to lowtemperature degradation of nano-Co₂O₃-doped 3Y-TZP was analyzed by X-ray diffraction. The microstructure of zirconia ceramic samples was determined by scanning electron microscopy, transmission electron microscopy, atomic force microscopy, and electron paramagnetic resonance studies. The addition of nano-Co₂O₃ into 3Y-TZP resulted in higher hydrothermal aging resistance than 3Y-TZP. The addition of 0.2 mol% nano-Co₂O₃ dopants resulted in the highest hydrothermal aging resistance among nano-Co₂O₃-doped 3Y-TZP ceramics. The grain sizes of 3Y-0.2Co are smaller than those in the control group. With the increase of cobaltous oxide doping contents, the segregation of Co3+ ions at the crystal boundary increased. The content of oxygen vacancies on the surface of the sample increased with the increase of the Co₂O₃ doping content. The oxygen vacancy concentrations

Shide Yu, Zhenyu Chen, Yiyin Sun: Foshan Stomatology Hospital & School of Medicine, Foshan University, Foshan, 528000, China

of 3Y-0.2Co increased obviously after aging. 3Y-0.1Co, 3Y-0.3Co, and the control showed decreased oxygen vacancy concentrations after aging. Trivalent element doping of 3Y-TZP effectively improved the aging resistance of 3Y-TZP. The addition of 0.2 mol% nano- Co_2O_3 resulted in the highest hydrothermal aging resistance. Improved aging resistance is attributed to the nano- Co_2O_3 doping resulting in the 3Y-TZP grain size inhibition, grain boundary segregation of cobalt ions, and oxygen vacancy maintenance. This work is expected to provide an effective reference for the development and application of budget dental materials by regulating grain boundary engineering.

Keywords: 3Y-TZP, low-temperature degradation, grain boundary segregation, doping, Co_2O_3

1 Introduction

3Y-TZP (3% yttria-stabilized tetragonal polycrystalline) has a high fracture toughness and strength and is widely used for hip prostheses ball-heads, dental implants, and dental prostheses [1–3]. However, when subjected to a humid and complex internal environment for an extended period, their surface will spontaneously transform into the martensitic phase [4,5]. The transformation of the tetragonal phase (t) to the monoclinic phase (m) will lead to surface microcracking and water molecules passing through these cracks and then penetrating the material, which leads to an obvious decrease in the mechanical properties of 3Y-TZP. This phenomenon is known as low-temperature degradation (LTD). The clinical survival rate of 3Y-TZP can thus be inevitably impacted in aqueous environments. For instance, hundreds of 3Y-TZP total hip prostheses ball-heads were reported to have failed between 1999 and 2000, which directly resulted in their withdrawal from the market [6,7]. Hydrothermal aging is a progressive process induced by water molecule invasion, starting from the surface and propagating

[#] These authors contributed equally to this work and should be considered co-first authors.

^{*} Corresponding author: Dahong Huang, Foshan Stomatology Hospital & School of Medicine, Foshan University, Foshan, 528000, China, e-mail: fshuangdh@126.com, tel: +86 18138316188

^{*} Corresponding author: Ting Sun, Foshan Stomatology Hospital & School of Medicine, Foshan University, Foshan, 528000, China, e-mail: sunting@jnu.edu.cn, tel: +86 13632444891

into the ceramic component, leading to microcracking and surface roughening [8,9].

Studies showed that doping of lower-valence oxides, such as Al₂O₃ and Co₂O₃, in 3Y-TZP is an effective method to improve its LTD performance since the doping of lower-valence oxides can stabilize zirconia in the cubic or tetragonal crystal structure [10,11]. Studies showed that doping of 3Y-TZP with a small amount of trivalent ions, *e.g.*, Al³⁺, Fe³⁺, Pr³⁺, Bi³⁺, and La³⁺, provides an adequate balance between aging resistance, mechanical properties, as well as aesthetics, *i.e.*, color and translucency [12–14].

Trivalent cations that segregate at the zirconia grain boundary can effectively retard the aging rate of 3Y-TZP ceramics without sacrificing the excellent mechanical properties [13]. The law of cation segregation at the boundary and its influence on the LTD effect of 3Y-TZP doped with trivalent cations of large radii, i.e., Sc³⁺, Nd³⁺, and La³⁺ have been primarily explored [15]. However, there is no data available for the hydrothermal aging behavior and the underlying mechanism for Co³⁺-doped 3Y-TZP. The large radii mismatch between the dopants and host cations is acknowledged as an essential driving force for the segregation at the grain boundary [13]. Since the mismatch between Co^{3+} (54.5 pm) and Zr^{4+} (84.0 pm) is large, Co^{3+} is expected to segregate obviously at the grain boundary which decrease the LTD susceptibility of 3Y-TZP ceramics. At the same time, Co₂O₃ is widely used as a colorant for clinically used dental 3-YTZP ceramics.

Moreover, from the perspective of the hydrothermal aging mechanism, the behavior of oxygen vacancies in 3Y-TZP ceramics should be evaluated to explain the varied hydrothermal aging kinetics. Although the mechanism of hydrothermal aging has not been completely recovered, studies showed that rapid annihilation of surface oxygen vacancies largely contributes to the hydrothermal aging of zirconia ceramics [16,17]. Reportedly, the oxygen vacancies adjacent to the Zr⁴⁺ ions might be a stabilizer for ZrO₂ of the tetragonal phase [18]. Additionally, it was shown that the activation energy of the aging kinetics (73–106 kJ·mol⁻¹) was comparable to that of ionic conductivity of 3Y-TZP ceramics below 500°C (88–89 kJ·mol⁻¹) [19]. Thus, it is commonly believed that the diffusion of water-derived species into the lattice of 3Y-TZP ceramics and the filling of oxygen vacancies (Vo) contributes to the aging process of 3Y-TZP ceramics [20].

Therefore, this study investigated the effect of the trivalent dopant's ionic radius on the LTD behavior in 3Y-TZP ceramics to understand the diffusion stabilization process of Co_2O_3 during the non-precursor transformation of 3Y-TZP. The hydrothermal aging kinetics of 3Y-TZP ceramics with a nano- Co_2O_3 dopant concentration of 0.1–0.3 mol%

were studied since the concentration of dopant also has a crucial influence on the aging kinetics of 3Y-TZP.

2 Materials and methods

2.1 Preparation of samples

The 3 mol% yttria-stabilized zirconia nanosized powder (3Y-TZP, TZ-3Y, purity > 99.9%, Tosoh, Japan) with approximately 0.1 wt% of additives, including SiO2, Fe2O3, NaO2 and Al₂O₃ was used. The specific surface area of 3Y-TZP ceramics is $16 \pm 3 \,\mathrm{m}^2 \,\mathrm{g}^{-1}$ and the mean particle diameter is 0.6 µm. The 3Y-TZP ceramic powders were mixed with nano-Co₂O₃ powders (purity > 99.999%, Aladdin) at concentrations of 0.1, 0.2, and 0.3 mol%, respectively. The mixed powders were added with ethanol as the mixing medium and were then milled in a Teflon jar for 24 h with 5 and 1 mm zirconia milling balls. Milled powders were dried in an oven to obtain 3Y-xCo powders at 80°C for 8 h and then cold isostatically pressed at 250 MPa for 2 min and pressure-less sintered in air at 1,450°C for 2 h. The constant heating and cooling rates were set as 3 and 10°C·min⁻¹, respectively. The sample blocks ($40 \times 40 \times 3$ mm) were then cut into 36 × 4 × 3 mm rods and then ground orderly with SiC papers of 120, 240, 600, 800, 1,200, 2,000, 3,000, 4,000, and 5,000 grades, and polished with 1 and 0.05 µm diamond pastes to obtain an optically reflective surface subsequently.

2.2 Assessment of aging kinetics

Polished samples (n=3) of each group were tested for LTD in deionized water for 10, 15, 20, and 30 h at 134°C and under a pressure of 2 bar in an autoclave. The amount of transformation in all specimens was measured by X-ray diffraction (XRD, Japan Smartlab) using Cu-K α radiation at 40 kV and 40 mA, a scan range of 20°–80° (2 θ), with a step size of $0.02 \, \mathrm{s}^{-1}$. Fractions of $m\text{-ZrO}_2$ and $t\text{-ZrO}_2$ were measured by the diffraction patterns in accordance with the method used by Garvie [21] and modified by Toraya [22]:

$$X_{\rm m} = \frac{I_{\rm m}(\bar{1}11) + I_{\rm m}(111)}{I_{\rm m}(\bar{1}11) + I_{\rm m}(111) + I_{\rm t}(101)},$$

where $X_{\rm m}$ is the relative amount of the monoclinic phase, and $I_{\rm m}$ and $I_{\rm t}$ are the intensities of the monoclinic and tetragonal peaks, respectively.

DE GRUYTER

The density of the eventual samples was tested in deionized water according to Archimedes' principle. The grain size distributions were obtained on polished surfaces after thermal etching at 1,350°C for 20 min. At least 1,000 grains were counted with NANO MEASURER 1.2.5 software, and the results were reported as average results (±standard deviation). The distribution of dopant cations (Co³⁺ and Y³⁺) near the grain boundaries was analyzed by scanning transmission electron microscopy (STEM, FEI Talos F200X, America), energy-dispersive X-ray spectroscopy (EDS), and high-angle annular dark-field detector in thin foils. ESR (ES-FA200, JEOL, Japan) was used to quantitatively detect the oxygen vacancies. Surface topography and roughness were determined using atomic force microscopy (AFM, MFP-3D-S, Asylum Research, USA). Electron paramagnetic resonance (EPR) measurements were recorded with an Xband CW-EPR Bruker EMX with a 100 kHz modulation frequency and a microwave power of 1 mW.

2.4 Characterization of mechanical properties

According to ISO 6872 [23], blocks were cut into $36 \times 4 \times 3 \text{ mm}^3$ test bars (n = 5) and the three-point bending strength was tested:

$$\sigma_{\rm t} = \frac{3FL}{2hd^2}$$

where F represents the maximum load, L represents the space of fixtures, b is the sample's width, and d is the sample's thickness.

The fracture toughness and Vickers hardness [24,25] were tested by micro-indentation. The indentations were

fabricated on the surfaces of samples of different compositions at 98.1 N, and the expected cracks originated at the corners of the indentation after loading. Indentations were imaged by scanning electron microscopy (SEM). The fracture toughness of apparent indentation was analyzed using the equation proposed by Niihara et al. [26].

2.5 Cell culture and cytotoxicity tests

Human oral epithelial cells (HOECs) were chosen to conduct the cytotoxicity experiments of doped 3Y-TZP. HOECs were cultured in Dulbecco's modified Eagle's medium containing 10% (v/v) heat-inactivated fetal bovine serum and antibiotics (100 µg·mL⁻¹ streptomycin and 100 IU·mL⁻¹ penicillin) for 24 h at 37°C in a humidified atmosphere with 5% CO_2 . Cells were seeded on each test substrate at 1×10^5 cells·mL⁻¹ in the same media for all assays. Untreated HOECs were set as control. The CCK-8 assay kit (Sangon Biotech, China) was used for the evaluation of cytotoxicity according to the manufacturer's instructions. About 10 µL of CCK-8 solution was added to each well. The plate was then incubated for 1h at 37°C, and the optical density at 450 nm was measured with a plate spectrophotometer (NanoDrop ND-1000, Thermo Scientific, Waltham, MA, USA). Measurements were made in triplicate for each sample and the mean values were recorded.

2.6 Statistical analysis

One-way analysis of variance with Tukey's post hoc test and Tukey's multiple comparisons test were employed in the statistical analysis. GraphPad Prism 8 software was

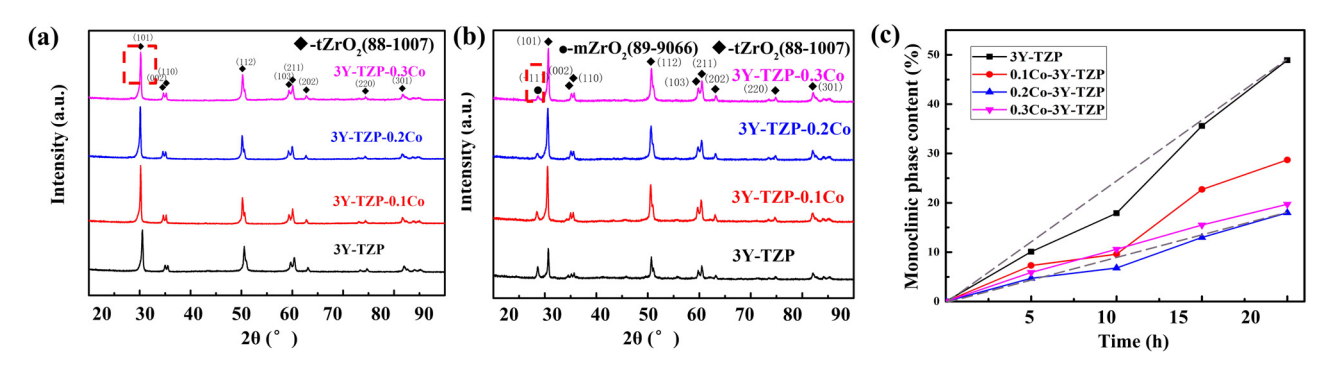


Figure 1: XRD diffraction patterns and the monoclinic phase content of Co_2O_3 -doped 3Y-TZP before and after hydrothermal degradation. (a) XRD diffraction patterns of 3Y-xCo (x = 0, 0.1, 0.2, 0.3 mol%) before aging. (b) XRD patterns of 3Y-xCo (x = 0, 0.1, 0.2, 0.3 mol%) after aging. (c) Monoclinic phase content of 3Y-xCo (x = 0, 0.1, 0.2, 0.3 mol%) after aging.

employed in the analysis, where α was set to 0.05. Mean values plus standard deviations are presented in the results, and different letters in the figures show statistical significance.

3 Results and discussion

3.1 Phase analysis

Figure 1a shows that before aging all samples consisted of $\rm ZrO_2$ of tetragonal phase regardless of doping of $\rm Co_2O_3$. Figure 1a shows the characteristics tetragonal peak ($I_{\rm m}$ (111)) at 2θ values of $\rm 30.2^{\circ}$ regardless of the amount of $\rm Co_2O_3$ dopants (see XRD analysis in Figure 1a). This revealed that doping of $\rm Co_2O_3$ in 3Y-TZP ceramics did not bring impurity and a second phase. After hydrothermal degradation for 20 h (Figure 1b and c), the control showed the highest monolithic peak ($I_{\rm m}$ (111)) and 3Y-0.2Co showed the lowest monolithic peak ($I_{\rm m}$ (111)) at 2θ values of 28.2°. Moreover, the 3Y-0.2Co samples showed the lowest monoclinic phase content than 3Y-0.1Co, 3Y-0.3Co, and the control group from 0 to 20 h in steam.

3.2 Microstructure observation

A density of ≥6.00 g·cm⁻³ is required for the application of 3Y-TZP ceramics as a load-bearing biomaterial [27]. The densification of doped 3Y-TZP ceramics is a challenge as

proved by studies that the addition of dopants such as La₂O₃ and Al₂O₃ significantly decreased the densification of 3Y-TZP ceramics [13]. However, the grain size of 3Y-xCo (x = 0.1, 0.2, 0.3 mol%) is smaller than the control group (P <0.05), indicating that doping of Co₂O₃ suppresses the grain growth. Densified surfaces with clear grain boundaries were also observed by SEM for sintered 3Y-TZP ceramics doped with Co₂O₃ that can be parallel to the 3Y-TZP ceramics (Figure 2). 3Y-xCo (x = 0.1, 0.2, 0.3 mol%) showed no statistically significant difference among the results of each group (P > 0.05). This verified that the dopants have a pinning effect at the grain boundary, thereby retarding the grain boundary mobility that can enhance the densification of 3Y-TZP and reduce the accumulation of water grain boundary [28]. Thus, Co₂O₃-doped 3Y-TZP ceramics are expected to exhibit higher mechanical strength for their densified surface structure and decreased grain size.

AFM images after hydrothermal degradation of 3Y-TZP-0.2Co (Figure 3a) showed that the phase transition from the tetragonal phase to the monoclinic phase of the first single grain on the surface triggered the phase transition of the adjacent grain, which eventually resulted in grain agglomerates and surface roughening. The surface of 3Y-TZP-0.2Co became rough with the vertical heights ranging from 7.6 to 23.2 nm 5 h after aging. Transmission electron microscopy (TEM) images of internal microscopic changes of crystals after hydrothermal degradation of 3Y-0.2Co (Figure 3b) revealed the presence of microcracks and intergranular fractures. The intergranular cracking accompanying the hydrothermal aging [12,27] clearly indicated the weakness of the grain boundary. Reportedly, after hydrothermal aging, the reduction of the ionic conductivity

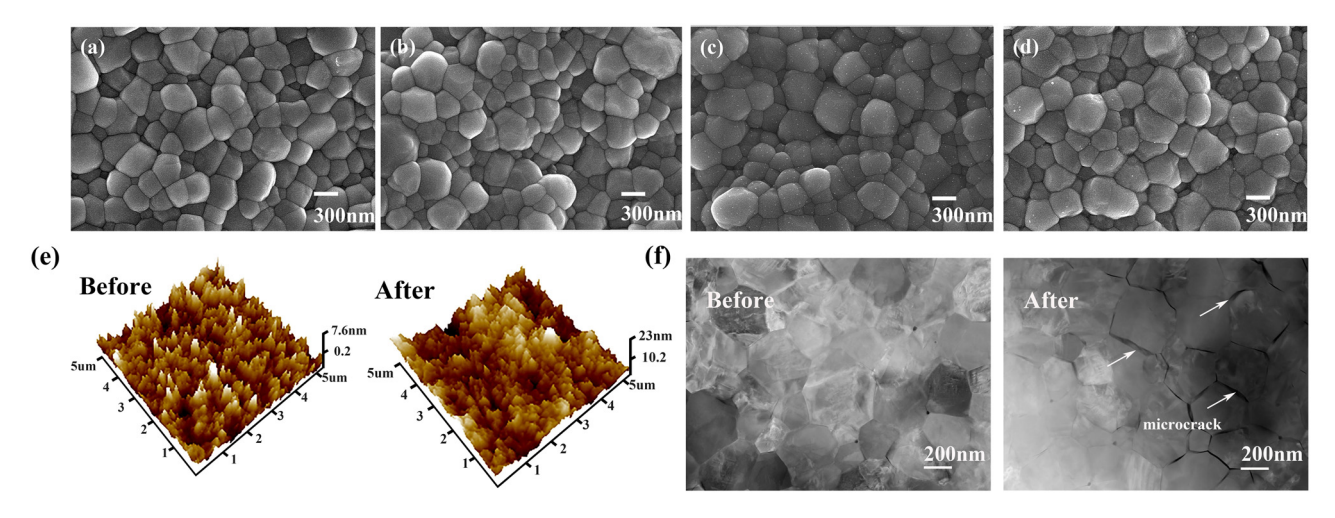


Figure 2: Microstructure observation of Co_2O_3 doped 3Y-TZP. (a–d) SEM patterns of 3Y-xCo (x = 0, 0.1, 0.2, 0.3 mol%). (e and f) Grain size distribution of 3Y-xCo (x = 0, 0.1, 0.2, 0.3 mol%). AFM (e) and HR-TEM (f) images of the surface and internal microscopic changes in crystals after hydrothermal degradation of 3Y-TZP-xCo (x = 0, 0.1, 0.2, 0.3 mol%).

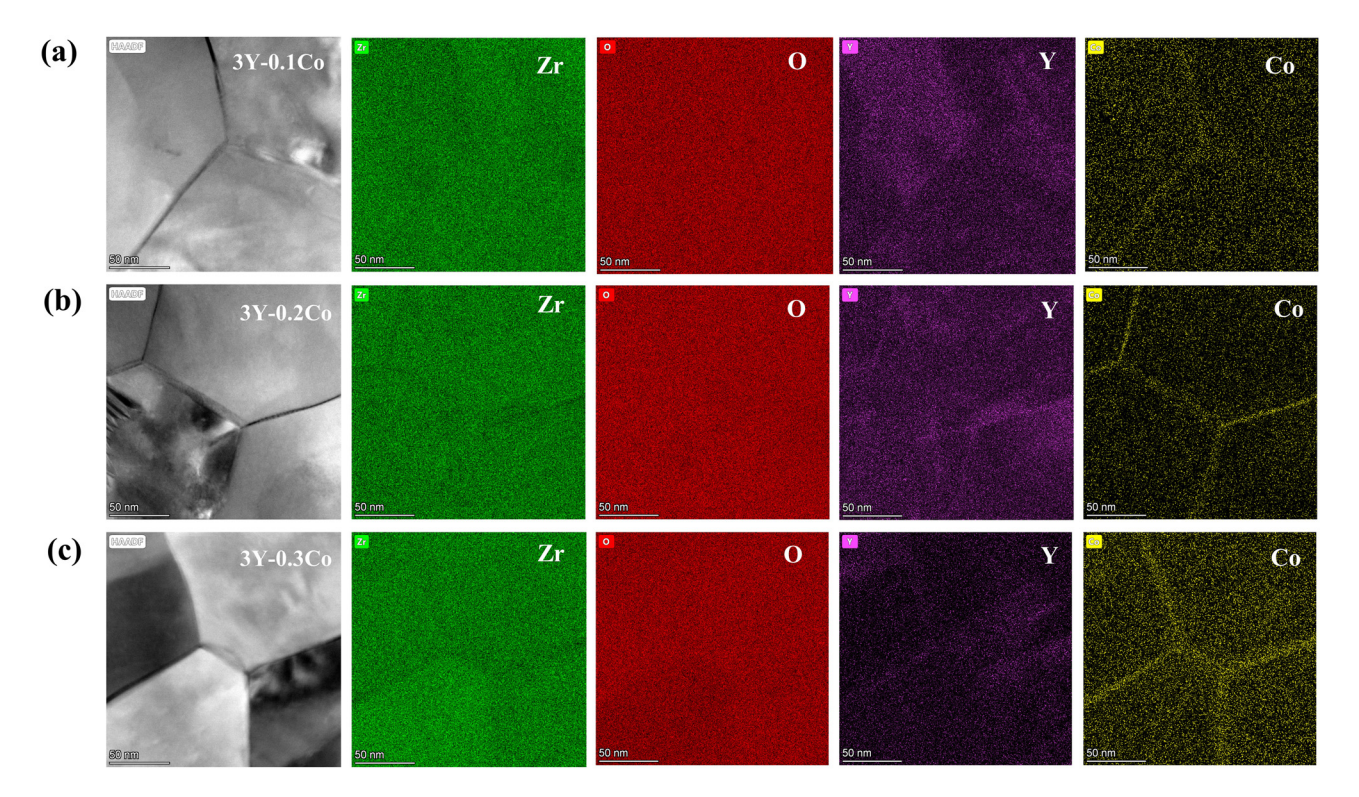


Figure 3: Grain boundary structure of Co_2O_3 .doped 3Y-TZP before hydrothermal degradation. (a) TEM observation of the grain boundary and EDS mapping of chemical ion distribution across the grain boundaries of 3Y-0.1Co. (b) TEM observation of the grain boundary and EDS mapping of chemical ion distribution across the grain boundaries of 3Y-0.2Co. (c) TEM observation of the grain boundary and EDS mapping of chemical ion distribution across the grain boundaries of 3Y-0.3Co.

in the grain boundary region was more severe than the reduction in the bulk area [29], revealing that grain boundary regions are active sites for hydrothermal aging.

3.3 Grain boundary segregation analysis

TEM and EDS energy spectrum mapping of 3Y-TZP-doped Co₂O₃ (Figures 3 and 4) showed Co³⁺ ions segregated at the grain boundaries, while Y3+ ions are evenly distributed at the grain boundaries both before and after aging degradation. Zr⁴⁺ and O²⁺ ions showed no segregation at the grain boundaries before aging. With the increase of doping of the Co₂O₃ content, the segregation of Co³⁺ ions increased. The concentration of segregated Co³⁺ ions was 1.2% for 3Y-0.1Co, 1.6% for 3Y-0.2Co, and 2.0% for 3Y-0.3Co after aging degradation (Figure 4). The mismatch in the cation size between Co3+ (54.5 pm) and Zr4+ ions (84.0 pm) is larger than that between Y³⁺ (90.0 pm) and Zr⁴⁺ ions, thus resulting in stronger grain boundary segregation behavior of Co₂O₃doped 3Y-TZP ceramics than 3Y-TZP [30]. Increased tetravalent element grain boundary segregation can strengthen the grain boundaries and inhibit the diffusion of water

molecules, therefore leading to excellent aging resistance of Co_2O_3 -doped 3Y-TZP ceramics. The ideal amount of dopant concentrations should be the maximum amount that can be dissolved at the zirconia grain boundaries after cooling without introducing a secondary phase. However, in this study, 3Y-0.2Co showed superior anti-aging behavior than 3Y-0.3Co. This can be explained as follows: the lattice parameters and constituent phases of the remaining ZrO_2 of the tetragonal phase also have a critical influence on the aging resistance of the 3Y-TZP ceramics added with dopants [17].

3.4 Oxygen vacancy analysis

EPR results (Figure 5) showed that the oxygen vacancy concentrations of 3Y-0.2Co increased obviously after aging. 3Y-0.1Co, 3Y-0.3Co, and the control showed decreased oxygen vacancy concentrations after aging. Previous studies have shown that rapid annihilation of surface oxygen vacancies is the main mechanism of hydrothermal aging degradation of zirconia ceramics [16,17]. Further study (Figure 5) showed that the content of oxygen vacancies on the surface of the sample varies with the increase of the Co_2O_3 doping content

6 — Shide Yu et al. DE GRUYTER

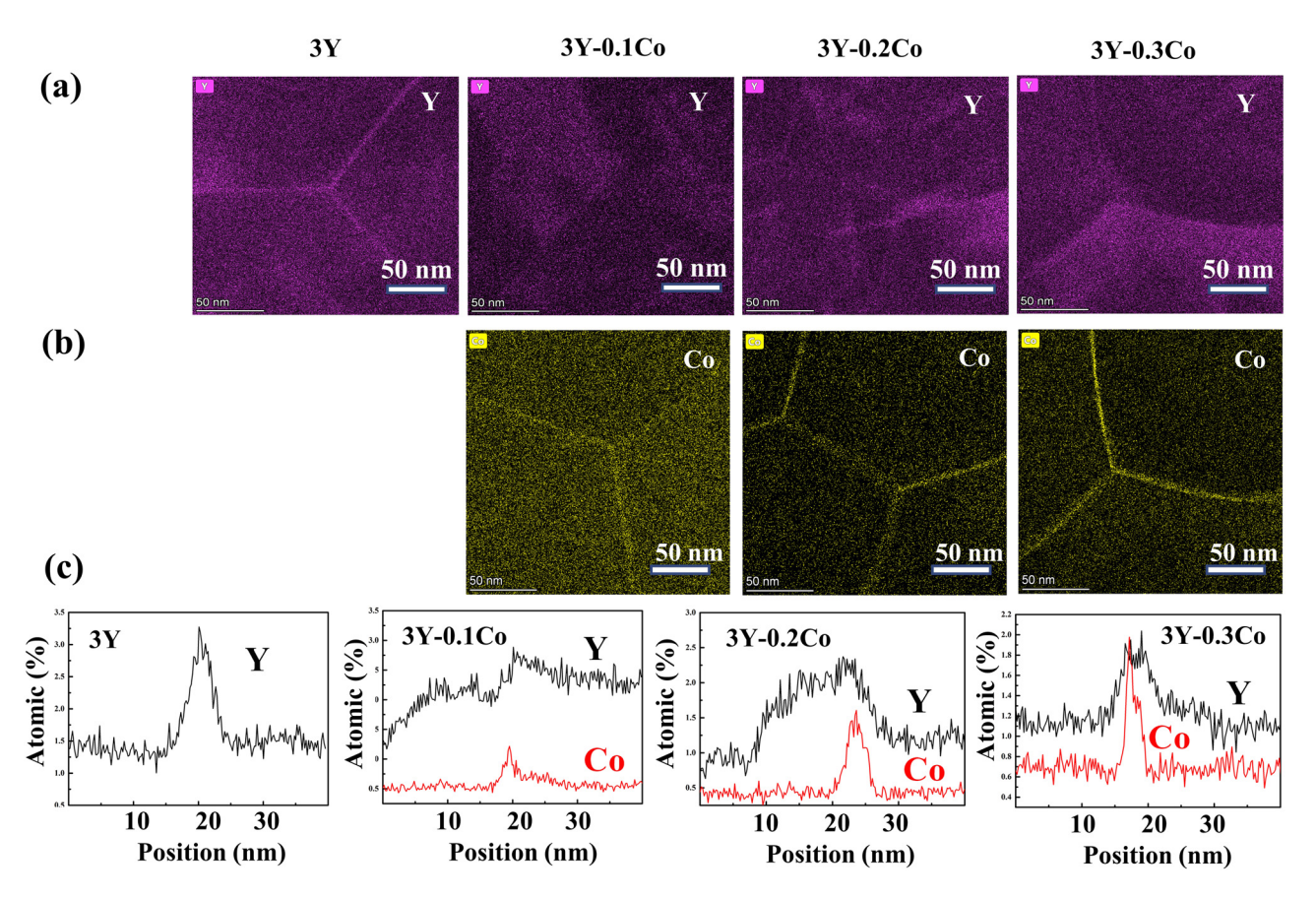


Figure 4: Grain boundary structure of Co_2O_3 -doped 3Y-TZP after hydrothermal degradation. (a) EDS mapping and Y^{3+} distribution across the grain boundaries of 3Y-xCo (x = 0, 0.1, 0.2, 0.3 mol%). (b) EDS mapping and corresponding chemical compositions of Co^{3+} across the grain boundaries of 3Y-xCo (x = 0, 0.1, 0.2, 0.3 mol%). (c) Percentage of deviated atoms of Co^{3+} ions before and after hydrothermal degradation of 3Y-xCo (x = 0, 0.1, 0.2, 0.3 mol%).

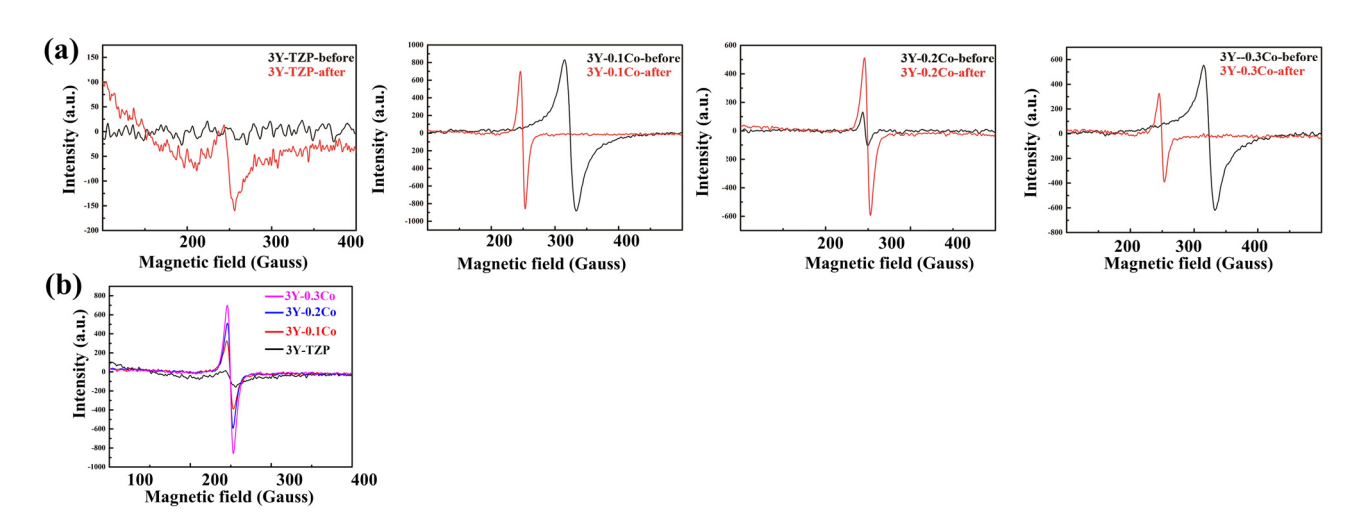


Figure 5: Oxygen vacancy characterization of Co_2O_3 -doped 3Y-TZP before and after hydrothermal degradation (EPR measurements were recorded with an X-band CW-EPR Bruker EMX with a 100 kHz modulation frequency and a microwave power of 1 mW). (a) Change in the oxygen vacancy content for 3Y-xCo (x = 0, 0.1, 0.2, 0.3 mol%) before and after hydrothermal degradation. (b) Characterization of oxygen vacancy of 3Y-xCo (x = 0, 0.1, 0.2, 0.3 mol%) after hydrothermal degradation.

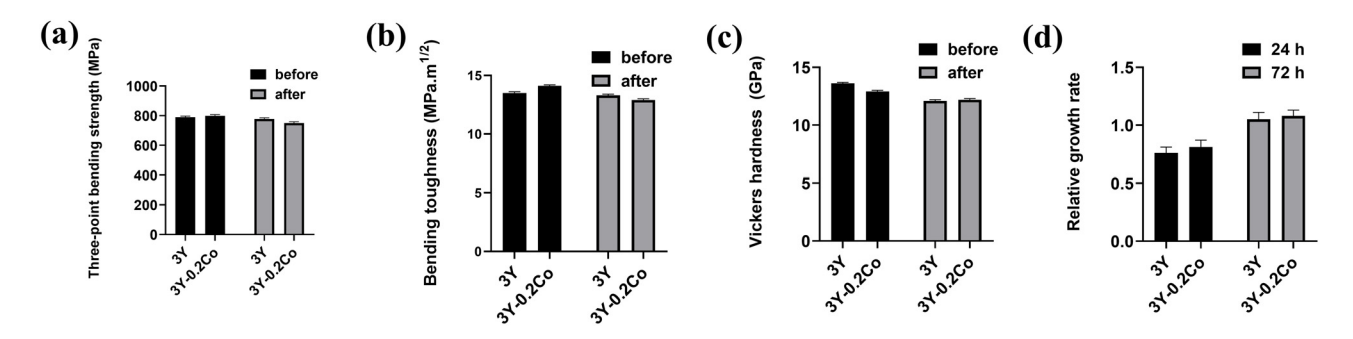


Figure 6: Mechanical properties and biocompatibility of 3Y-0.2Co before and after hydrothermal degradation. (a) Three-point bending strength of 3Y-0.2Co; (b) the Vickers hardness of 3Y-0.2Co; (c) fracture toughness of 3Y-0.2Co; and (d) Proliferation of oral epithelial cells on 3Y-0.2Co.

and further verified that changes in oxygen vacancy of 3Y-TZP samples resulted from doping of Co₂O₃. This result is in accordance with previous studies that the doping of oxide of low valence states (divalent and trivalent cations) can maintain oxygen vacancies of 3Y-TZP ceramics [31] since the segregated cations can bind to the oxygen vacancies at the grain boundary and obviously interrupt the annihilation of oxygen vacancies [13]. The filling of oxygen vacancies by "water-derived species" at the grain boundary is found to induce the hydrothermal aging of 3Y-TZP ceramics [20]. Thus, the oxygen vacancy concentration has a direct influence on the aging kinetics of 3Y-TZP ceramics for the ionic resistivity and is given by[32]

$$\rho = \frac{1}{2\mu[Vo"]F}.$$

Here, μ is the mobility of the oxygen vacancy, [Vo"] is the oxygen vacancy concentration and F is the Faraday constant. A higher concentration of oxygen vacancies at the grain boundary leads to a higher aging resistance of 3Y-TZP ceramics. Moreover, smaller undersized dopant cations (such as Al³⁺ and Co³⁺) retard the aging process well due to their stronger bonding of the oxygen vacancy [13,33]. Thus, maintaining the oxygen vacancy induced by doping of Co₂O₃ improved the aging resistance of 3Y-TZP ceramics. The highest aging resistance of 3Y-0.2Co among all tested samples is mainly attributed to their maintained oxygen vacancy concentrations.

Based on the above results, improved aging resistance is attributed to tCo₂O₃ doping resulting in 3Y-TZP grain size inhibition, grain boundary segregation of Co³⁺ irons, and oxygen vacancy maintenance. Not only the type of dopant but also the amount of dopant was crucial for designing aging-resistant 3Y-TZP ceramics. The hydrothermal aging behavior suggested that 3Y-0.2Co displayed greater aging resistance than 3Y-0.1Co, 3Y-0.3Co, and the control group, which corresponded to 0-60 years in the human body [34].

3.5 Mechanical properties

Currently, maintaining the mechanical strength of 3Y-TZP ceramics after adding cation dopants is a challenge. For instance, a previous study confirmed the addition of 3Y-TZP ceramics with a small amount of La³⁺ dopants to statistically decrease the mechanical strength of 3Y-TZP ceramics [35], although it improved the aesthetic appearance for dental applications. However, the three-point bending strength, the fracture toughness and Vickers hardness (Figure 6a-c) were not significantly different for 3Y-0.2Co and the control (P < 0.05) both before and after aging, indicating that the addition of Co cation dopants into 3Y-TZP did not decrease the mechanical strength of 3Y-TZP both before and after aging.

3.6 Biocompatibility

CCK-8 results (Figure 6d) showed that hydrothermal aging had no impact on the cytotoxicity of 3Y-0.2Co and the control (P > 0.05). The cytotoxicity of 3Y-0.2Co and the control were not statistically different both before and after aging (P > 0.05). This revealed that the addition of trivalent cation dopants into 3Y-TZP did not decrease the biocompatibility of 3Y-TZP both before and after aging. Reportedly, Co was safe towards the normal cells [36]. Adequate Co ion release could facilitate angiogenesis [37]. Furthermore, as shown in Figures 3-5, 3Y-0.2Co composites have good phase stability, which will not accelerate the release of Co ions and cause biotoxicity.

4 Conclusion

The present investigation has shown that nano trivalent oxide (Co₂O₃) dopants at concentrations from 0.1 to $0.3 \, \text{mol}\%$ improved the aging resistance of 3Y-TZP ceramics. The addition of $0.2 \, \text{mol}\%$ of Co_2O_3 resulted in the highest hydrothermal aging resistance. Improved aging resistance is attributed to the Co_2O_3 doping resulting in 3Y-TZP grain size inhibition, grain boundary segregation of cobalt ions, and oxygen vacancy maintenance. This study provides theoretical guidance for reasonable dopant alterations and possible methods to decrease LTD susceptibility of 3Y-TZP in clinics.

Funding information: This work was supported by the Guangdong Medical Science and Technology Research Fund Project (A2022358) and Natural Science Foundation of Guangdong Province (2019A1515010263).

Author contributions: All authors have accepted responsibility for the entire content of this manuscript and approved its submission.

Conflict of interest: The authors state no conflict of interest.

References

- [1] Tovar-Vargas, D., B. Ferrari, A. J. Sanchez-Herencia, M. Anglada, and E. Jimenez-Pique. Low temperature degradation and mechanical properties of alumina reinforced ceria-zirconia by colloidal processing. *Journal of the European Ceramic Society*, Vol. 41, No. 2, 2021, pp. 1459–1470.
- [2] Sun, T., X. Liu, X. Zhan, L. Ou, and R. Lai. Hepatic distribution and toxicity of zirconia nanoparticles in vivo and in vitro. *Process Safety and Environmental Protection*, Vol. 147, 2021, pp. 134–145.
- [3] Sun, T., Y. Kang, J. Liu, Y. Zhang, L. Ou, X. Liu, et al. Nanomaterials and hepatic disease: toxicokinetics, disease types, intrinsic mechanisms, liver susceptibility, and influencing factors. *Journal of nanobiotechnology*, Vol. 19, No. 1, 2021, id. 108.
- [4] Nishihara, H., M. H. Adanez, and W. Att. Current status of zirconia implants in dentistry: Preclinical tests. *Journal of Prosthodontic Research*, Vol. 63, No. 1, 2019, pp. 1–14.
- [5] Sun, T., R. Liu, X. Liu, X. Feng, Y. Zhang, and R. Lai. The biocompatibility of dental graded nano-glass-zirconia material after aging. Nanoscale Research Letters, Vol. 13, No. 1, 2018, id. 61.
- [6] Chevalier, J. What future for zirconia as a biomaterial? *Biomaterials*, Vol. 27, No. 4, 2006, pp. 535–543.
- [7] Masonis, J. L., R. B. Bourne, M. D. Ries, R. W. McCalden, A. Salehi, and D. C. Kelman. Zirconia femoral head fractures: A clinical and retrieval analysis. *The Journal of arthroplasty*, Vol. 19, No. 7, 2004, pp. 898–905
- [8] Ban, S. Chemical durability of high translucent dental zirconia. Dental materials journal, Vol. 39, No. 1, 2020, pp. 12–23.
- [9] Badarneh, A., J. J. Eun Choi, K. Lyons, G. Porter, N. Waddell, and K. Chun Li. The effect of aging on the wear performance of monolithic zirconia. *Dental Materials: Official Publication of the Academy of Dental Materials*, Vol. 38, No. 5, 2022, pp. e136–e146.

- [10] Takigawa, Y., T. Shibano, Y. Kanzawa, and K. Higashi. Effect of small amount of insoluble dopant on tetragonal to monoclinic phase transformation in tetragonal zirconia polycrystal. *Materials Transactions*, Vol. 50, No. 5, 2009, pp. 1091–1095.
- [11] Kumar, C. S., R. Bauri, and G. S. Reddy. Phase stability and conductivity of rare earth co-doped nanocrystalline zirconia electrolytes for solid oxide fuel cells. *Journal of Alloys and Compounds*, Vol. 833, 2020, id. 155100.
- [12] Samodurova, A., A. Kocjan, M. V. Swain, and T. Kosmač. The combined effect of alumina and silica co-doping on the ageing resistance of 3Y-TZP bioceramics. *Acta Biomaterialia*, Vol. 11, 2015, pp. 477–487.
- [13] Zhang, F., K. Vanmeensel, M. Batuk, J. Hadermann, M. Inokoshi, B. Van Meerbeek, et al. Highly-translucent, strong and agingresistant 3Y-TZP ceramics for dental restoration by grain boundary segregation. *Acta Biomaterialia*, Vol. 16, 2015, pp. 215–222.
- [14] Ramesh, S., K. S. Lee, and C. Tan. A review on the hydrothermal ageing behaviour of Y-TZP ceramics. *Ceramics International*, Vol. 44, No. 17, 2018, pp. 20620–20634.
- [15] Khan, M., S. Ramesh, L. Bang, Y. Wong, S. Ubenthiran, C. Tan, et al. Effect of copper oxide and manganese oxide on properties and low temperature degradation of sintered Y-TZP ceramic. *Journal of Materials Engineering and Performance*, Vol. 23, No. 12, 2014, pp. 4328–4335.
- [16] Pandoleon, P., E. Kontonasaki, N. Kantiranis, N. Pliatsikas, P. Patsalas, L. Papadopoulou, et al. Aging of 3Y-TZP dental zirconia and yttrium depletion. *Dental Materials: Official Publication of the Academy of Dental Materials*, Vol. 33, No. 11, 2017, pp. e385–e392.
- [17] Zhang, F., M. Batuk, J. Hadermann, G. Manfredi, A. Mariën, K. Vanmeensel, et al. Effect of cation dopant radius on the hydrothermal stability of tetragonal zirconia: Grain boundary segregation and oxygen vacancy annihilation. *Acta Materialia*, Vol. 106, 2016, pp. 48–58.
- [18] Fabris, S., A. T. Paxton, and M. W. Finnis. A stabilization mechanism of zirconia based on oxygen vacancies only. *Acta Materialia*, Vol. 50, No. 20, 2002, pp. 5171–5178.
- [19] Fabbri, P., C. Piconi, E. Burresi, G. Magnani, F. Mazzanti, and C. Mingazzini. Lifetime estimation of a zirconia-alumina composite for biomedical applications. *Dental Materials: Official Publication* of the Academy of Dental Materials, Vol. 30, No. 2, 2014, pp. 138–142.
- [20] Pezzotti, G., M. C. Munisso, A. A. Porporati, and K. Lessnau. On the role of oxygen vacancies and lattice strain in the tetragonal to monoclinic transformation in alumina/zirconia composites and improved environmental stability. *Biomaterials*, Vol. 31, No. 27, 2010. pp. 6901–6908.
- [21] de Paula Miranda, R. B., T. P. Leite, A. C. F. Pedroni, M. M. Marques, N. B. de Lima, J. Marchi, et al. Effect of titania addition and sintering temperature on the microstructure, optical, mechanical and biological properties of the Y-TZP/TiO(2) composite. *Dental Materials:* Official Publication of the Academy of Dental Materials, Vol. 36, No. 11, 2020, pp. 1418–1429.
- [22] Chen, T., S. Tekeli, R. P. Dillon, and M. L. Mecartney. Phase stability, microstructural evolution and room temperature mechanical properties of TiO2 doped 8 mol% Y2O3 stabilized ZrO2 (8Y-CSZ). *Ceramics International*, Vol. 34, No. 2, 2008, pp. 365–370.
- [23] Standardization IOf. ISO 6872: 2008. Dentistry: Ceramic materials. ISO Geneva; 2008.
- [24] Quinn, G. D. and R. C. Bradt. On the Vickers indentation fracture toughness test. *Journal of the American Ceramic Society*, Vol. 90, No. 3, 2007, pp. 673–680.

- [25] Furtado de Mendonca, A., M. Shahmoradi, C. V. D. Gouvêa, G. M. De Souza, and A. Ellakwa. Microstructural and mechanical characterization of CAD/CAM materials for monolithic dental restorations. *Journal of prosthodontics: Official Journal of the American College of Prosthodontists*, Vol. 28, No. 2, 2019, pp. e587–e594.
- [26] Niihara, K., R. Morena, and D. Hasselman. Evaluation of K Ic of brittle solids by the indentation method with low crack-to-indent ratios. *Journal of Materials Science Letters*, Vol. 1, 1982, pp. 13–16.
- [27] Xu, S., X. Tan, F. Liu, L. Zhang, Y. Huang, B. A. Goodman, et al. Growth and optical properties of thulia-doped cubic yttria stabilized zirconia single crystals. *Ceramics International*, Vol. 45, No. 13, 2019, pp. 15974–15979.
- [28] Hallmann, L., A. Mehl, P. Ulmer, E. Reusser, J. Stadler, R. Zenobi, et al. The influence of grain size on low-temperature degradation of dental zirconia. *Journal of Biomedical Materials Research Part B, Applied Biomaterials*, Vol. 100, No. 2, 2012, pp. 447–456.
- [29] Bowen, C., S. Ramesh, C. Gill, and S. Lawson. Impedance spectroscopy of CuO-doped Y-TZP ceramics. *Journal of Materials Science*, Vol. 33, 1998, pp. 5103–5110.
- [30] Chen, I.-W. Mobility control of ceramic grain boundaries and interfaces. *Materials Science and Engineering: A*, Vol. 166, No. 1–2, 1993, pp. 51–58.
- [31] Stepanov, S., O. Khasanov, E. Dvilis, V. Paygin, D. Valiev, and M. Ferrari. Luminescence performance of yttrium-stabilized zirconia

- ceramics doped with Eu3+ ions fabricated by Spark Plasma Sintering technique. *Ceramics International*, Vol. 47, No. 5, 2021, pp. 6608–6613.
- [32] Guo, X. Hydrothermal degradation mechanism of tetragonal zirconia. *Journal of Materials Science*, Vol. 36, 2001, pp. 3737–3744.
- [33] Nogiwa-Valdez, A. A., W. M. Rainforth, P. Zeng, and I. M. Ross. Deceleration of hydrothermal degradation of 3Y-TZP by alumina and lanthana co-doping. *Acta Biomaterialia*, Vol. 9, No. 4, 2013, pp. 6226–6235.
- [34] Gremillard, L., J. Chevalier, T. Epicier, and G. Fantozzi. Improving the durability of a biomedical-grade zirconia ceramic by the addition of silica. *Journal of the American Ceramic Society*, Vol. 85, No. 2, 2002, pp. 401–407.
- [35] Chevalier, J., L. Gremillard, A. V. Virkar, and D. R. Clarke. The tetragonal-monoclinic transformation in zirconia: lessons learned and future trends. *Journal of the American Ceramic Society*, Vol. 92, No. 9, 2009, pp. 1901–1920.
- [36] Ansari, S., R. Bhor, K. Pai, D. Sen, S. Mazumder, K. Ghosh, et al. Cobalt nanoparticles for biomedical applications: Facile synthesis, physiochemical characterization, cytotoxicity behavior and biocompatibility. *Applied Surface Science*, Vol. 414, 2017, pp. 171–187.
- [37] Baino, F., M. Montazerian, and E. Verné. Cobalt-doped bioactive glasses for biomedical applications: A review. *Materials*,, Vol. 16, No. 14, 2023, p. 4994.